JOURNAL OF THEORETICAL AND APPLIED MECHANICS
43, 3, pp. 609-630, Warsaw 2005

STABILITY OF ACTIVELY CONTROLLED ROTATING SHAFT MADE OF FUNCTIONALLY GRADED MATERIAL

Piotr M. Przybyłowicz

Institute of Machine Design Fundamentals, Warsaw University of Technology
e-mail: piotrp@ipbm.simr.pw.edu.pl

In the paper, the problem of active stabilisation of a rotating shaft made of a three-phase Functionally Graded Material (FGM) with piezoelectric fraction is presented. Due to internal friction, at a certain critical rotation speed, the shaft loses its stability and starts to vibrate in a self-excited manner. In the paper, a method protecting the system from such a phenomenon by making use of a FGM controlled by electrodes bonded and embedded in the structure of the shaft is discussed in detail. The critical threshold is found by examination of the eigenvalues corresponding to linear formulas derived via uni-modal Galerkin's discretisation of partial differential equations of motion. The main goal of the paper is determination of such a distribution of the volume fraction of the active phase within the shaft, which makes the system possibly most resistant to self-excitation on the one hand, and still attractive in terms of strength properties on the other. The results are presented in the form of diagrams depicting the critical rotation speed vs. exponents describing volume distribution of the active phase as well as gain factors applied in the control system.

Key words: rotating shaft, stabilisation, functionally graded material, piezoceramic

1. Introduction

Rotating shafts, even when perfectly balanced, exhibit self-excited vibration brought about by internal dissipation due to damping in the material, structural friction in articulated joints, supports, etc. The instability occurs due to exceeding the critical rotation speed (over the first eigenfrequency corresponding to flexural vibration of the given shaft as a beam), and is manifested by sudden growth in the amplitude of transverse vibration for a slight change

of the rotation speed. It is to be emphasised that the mentioned critical speed is definitely different from that classically understood and being related to the resonance of rotors undergoing excitation by unbalanced inertia, see Kurnik (1992).

The last several years have been characterized by animated interest of scientific researchers and engineers in the so-called smart materials and structures which, in contradistinction to the classical ones, can adapt their properties to varying operating conditions according to the given algorithm. Smart systems combine mechanical properties with non-mechanical ones, most often with electric, magnetic, thermal, or sometimes, optical fields of interaction. The most popular smart structures employ elements controllable by easy-to-transduce electric signals. Predominantly, piezoelectric elements made of lead zirconate titanate (PZT) or polyvinylidene fluoride (PVDF) are applied.

Despite good electromechanical properties of piezoelectric ceramics, the surface-bonded actuators are brittle, heavy, non-flexible and non-conformable elements. Their alternatives, PVDF copolymers are, admittedly, flexible and conformable to any shape but they exhibit high electrical losses, are difficult to pole and their properties are sensitive to temperature variation. Instead of looking for an entirely new class of piezoelectric materials without the above-mentioned drawbacks, a concept of piezoelectric composites came into being (Newnham et al., 1980). First patterns of diphasic materials and several different piezocomposites were fabricated at the Pennsylvania State University. Properties of ceramic/polymer composites can be tailored by changing connectivity of the phases, volume fraction of the active component and spatial distribution of the ceramic phase. Piezocomposites exhibit excellent electromechanical properties and limit the detrimental characteristics of monoliths at the same time. In literature, one can come across various techniques used to form a variety of novel piezoceramic/polymer composites. Among them, the Solid Freeform Fabrication (SFF) containing Fused Deposition of Ceramics (FDC) and Sanders Prototype (SP) are most popular. The FDC or the lost mould endows piezocomposites with particularly good electromechanical properties. That way, Volume Fraction Gradients (VGFs), staggered rods, radial tubes, curved transducers and many other composite structures are fabricated (Safari, 1999).

The concept of piezoelectric stabilization of rotating shafts was described by Przybyłowicz (2002a), who investigated the efficiency of using piezoelectric actuators glued around the perimeter of the shaft. Recent developments in the field of smart structures and the coming of active composites into being have opened new possibilities to the control of rotating shafts. Composite ro-

tors, due to low specific weight, anisotropic properties and excellent torsional stiffness became competitive materials as compared to their traditional steel counterparts. The application of active piezoelectric fibers made them competitive even more. Efficient use of PFCs in rotating structures was confirmed by Kurnik and Przybyłowicz (2003).

The latest advances in material science have led to the emergence of a new class of smart materials, called functionally graded materials (FGMs). Their main feature, i.e. spatial variation of the microstructure endows such structures with optimal mechanical, electrical and thermal properties. In particular, FGMs are an answer to the electro- elastic mismatch between a passive host structure and piezoelectric actuator attached to its surface (Tylikowski, 2001). It is achieved through continuous gradation of volume fraction of constituent phases. FGMs are superior to the conventional smart materials because of lack of internal stress concentrations and interfacial debonding, which makes them have improved lifetime and reliability with respect to traditional structures, Liew *et al.* (2003).

This paper is concerned with active flutter suppression of a rotating shaft, i.e. stabilization and reduction of transverse vibration by making use of an active, functionally graded material containing three phases: two structural phases (traditional passive materials - carrying layer of aluminium and insulating layer of a polymer) and an active one (piezoceramic). The three constituents are a mixture of continuously varying volume fraction, see Fig. 1. The active phase is able to produce mechanical stress and strain under an electric field, which stabilizes operation of the rotating shaft if properly controlled. It occurs that the application of only three actuating electrodes around the shaft circumference is enough to generate a constant counter-bending moment despite rotary motion of the entire structure, see Przybylowicz (2002b). Such a moment opposes the internal interactions in the shaft that lead directly to self-excitation while exceeding the critical angular velocity.

A quite detailed discussion on rotating shafts was given by Librescu *et al.* (2005) who studied spinning thin-walled beams made of FGMs. They thoroughly examined the influence of a temperature field as well as an axial force on stability and evolution of the first natural frequency of circular cylindrical shafts. Their systems remained passive, however. In this work, the author's effort is focused on "active" aspects of such systems if manufactured with "smart" components integrally immersed in the entire FGM structure.

In the paper, the effect of radial distribution of components constituting the internal structure of a rotating shaft on the critical rotation speed is investigated. The shaft consists of three components, among which one of them

(the inner surface) comprises active piezoceramic (PZT) fraction. The stability is examined in terms of eigenvalues corresponding to equations of motion linearized around the trivial equilibrium position. The governing equations include terms describing internal friction in the shaft material as well as the control strategy based on the velocity feedback. Results of numerical simulations on the formulated model indicate considerable growth of the rotation speed at which the structure loses its stability.

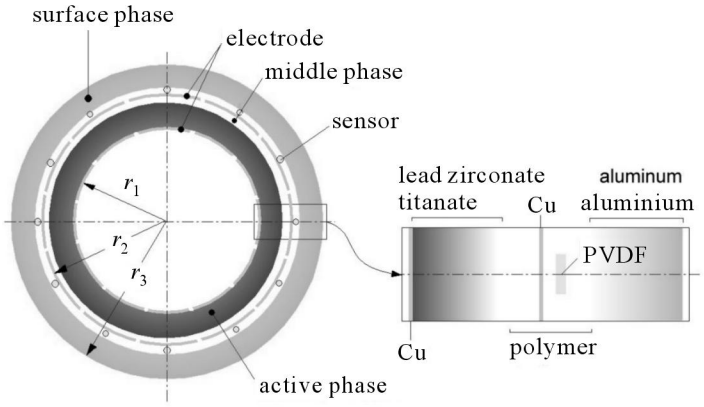

Fig. 1. A shaft made of a three-phase functionally graded material

2. Properties of the three-phase FGM structure

Consider a slender shaft rotating with a constant angular velocity ω around the vertical axis. The shaft is entirely made of a three-phase functionally graded material being a composition of an active constituent, which is a piezoceramic PZT, and two passive ones metallic (carrying) and polymeric (insulating). These components are mixed through the shaft thickness and their fraction in a certain point along the radius varies exponentially according to the following rules

$$\xi^1_{\rm pol} = \Big(\frac{r - r_1}{r_2 - r_1}\Big)^n \qquad \xi^2_{\rm pol} = \Big(\frac{r_3 - r}{r_3 - r_2}\Big)^n \tag{2.1}$$

where n is the assumed exponent of the applied distribution, $\xi^1_{\rm pol}$ denotes volume fraction of the polymeric constituent within the inner part of the shaft cross-section, i.e. between pure piezoceramic and pure polymer: $r \in (r_1, r_2)$, see also Fig. 1. Obviously, $\xi^2_{\rm pol}$ is the volume fraction in the outer part, between

the polymer and aluminium: $r \in (r_2, r_3)$. Accordingly, the effective Young's modulus, effective coefficient of internal friction (the damping described by the Kelvin-Voigt rheological model) as well as effective constant of electromechanical coupling in the piezoceramic-polymer phase are given by the following formulas and corresponding figures (Fig. 2 and Fig. 3)

$$Y_{ef} = \begin{cases} Y_{\mathrm{PZT}}(1-\xi^1_{\mathrm{pol}}) + Y_{\mathrm{pol}}\xi^1_{\mathrm{pol}} & \text{for} \quad r_1 < r < r_2 \\ Y_{\mathrm{Al}}(1-\xi^2_{\mathrm{pol}}) + Y_{\mathrm{pol}}\xi^2_{\mathrm{pol}} & \text{for} \quad r_2 < r < r_3 \end{cases} \tag{2.2}$$

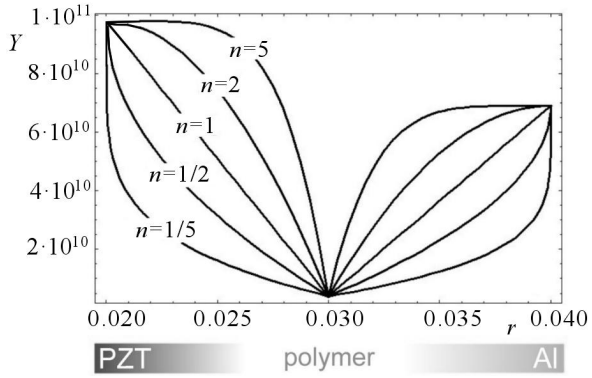

Fig. 2. Effective Young's modulus vs. radial coordinate of the shaft and some selected exponents n describing the function type of volume fraction

$$\beta_{ef} = \begin{cases} \beta_{\mathrm{PZT}}(1-\xi^1_{\mathrm{pol}}) + \beta_{\mathrm{pol}}\xi^1_{\mathrm{pol}} & \text{for} \quad r_1 < r < r_2 \\ \beta_{\mathrm{Al}}(1-\xi^2_{\mathrm{pol}}) + \beta_{\mathrm{pol}}\xi^2_{\mathrm{pol}} & \text{for} \quad r_2 < r < r_3 \end{cases} \tag{2.3}$$

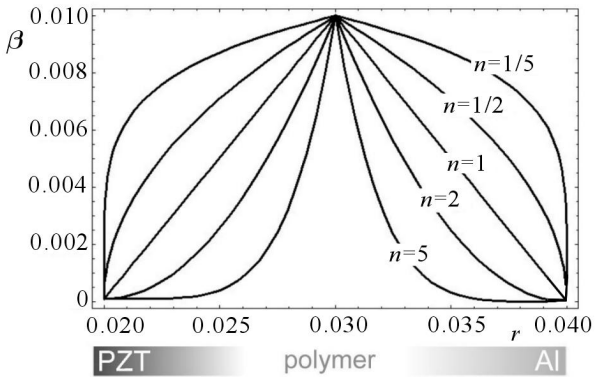

Fig. 3. Effective internal damping

$$d_{31}^{ef} = \begin{cases} d_{31}(1-\xi_{\text{pol}}^{1}) & \text{for} \quad r_1 < r < r_2 \\ 0 & \text{for} \quad r_2 < r < r_3 \end{cases} \tag{2.4}$$

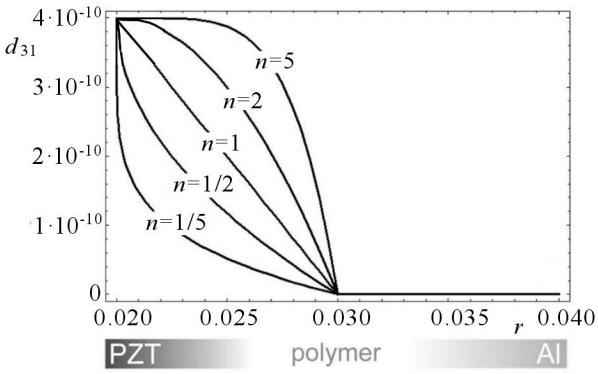

Fig. 4. Effective electromechanical coupling

3. Equations of motion of the shaft

In this Section, equations of motion of a rotating shaft made of a Functionally Graded Material exhibiting some features describing internal friction within the material will be derived. Assuming Kirchhoff's simplification and the fact that the deflection of the geometric axis remains plane, consider now the balance of internal forces and moments shown in Fig. 5 in order to find equations of dynamic equilibrium in both transverse directions (y and z) of the analysed shaft.

These equations are

$$\rho A \frac{\partial^2 y}{\partial t^2} = -\frac{\partial T_y}{\partial x} \qquad \rho A \frac{\partial^2 z}{\partial t^2} = -\frac{\partial T_z}{\partial x} \tag{3.1}$$

provided that the shaft is treated as a beam undergoing pure bending. In (3.1) ρ denotes the mass density of the FGM structure averaged over the cross-section area A, furthermore: y, z are transverse coordinates and T_y, T_z – components of the shear force. By balancing the moments, one concludes

$$\begin{bmatrix} T_y \\ T_z \end{bmatrix} = \frac{\partial}{\partial x} \begin{bmatrix} M_z \\ M_y \end{bmatrix} \tag{3.2}$$

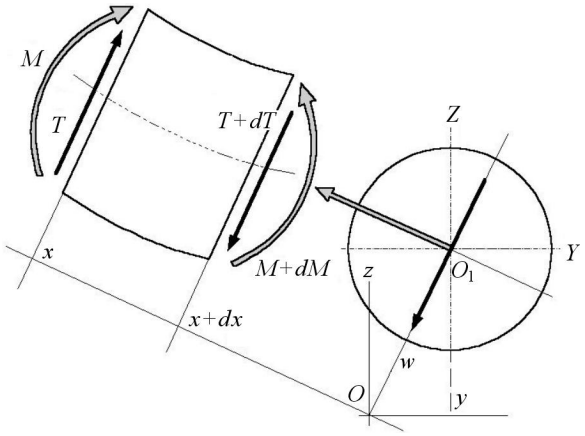

Fig. 5. Bending moments and transverse forces acting on an infinitesimal element of the shaft

Naturally, the bending moments are normal stresses multiplied by respective coordinates and integrated over the entire cross-section of the shaft

$$M_z = \int\limits_A \sigma y \, dA \qquad\qquad M_y = \int\limits_A \sigma z \, dA \tag{3.3}$$

The stress itself obeys Hooke's law, here completed with terms describing the presence of internal damping expressed by the Kelvin-Voigt rheological model

$$\begin{aligned} \sigma &= Y_{ef}\Big(1 + \beta_{ef}\frac{\partial}{\partial t}\Big)(\kappa_y y + \kappa_z z) = \\ &= Y_{ef}(\kappa_y y + \kappa_z z) + Y_{ef}\beta_{ef}(\dot{\kappa}_y y + \kappa_y \dot{y} + \dot{\kappa}_z z + \kappa_z \dot{z}) \end{aligned} \tag{3.4}$$

where κ_y and κ_z are curvatures in the xy and xz plane, respectively. Knowing that components of circumferential velocity of a given point in the cross-section of the shaft $\boldsymbol{v} = \boldsymbol{\omega} \times \boldsymbol{r}$, i.e.

$$\begin{bmatrix} \dot{x} \\ \dot{y} \\ \dot{z} \end{bmatrix} = \begin{vmatrix} \boldsymbol{i} & \boldsymbol{j} & \boldsymbol{k} \\ \omega & 0 & 0 \\ x & y & z \end{vmatrix} \Rightarrow \dot{y} = -\omega z \qquad \text{and } \dot{z} = \omega y \tag{3.5}$$

Substituting the above formulas into integrals (3.3), one obtains

$$\begin{aligned} M_z &= \kappa_y \int\limits_A Y_{ef} y^2 \, dA + (\dot{\kappa}_y + \omega \kappa_z) \int\limits_A \beta_{ef} Y_{ef} y^2 \, dA \\ M_y &= \kappa_z \int\limits_A Y_{ef} z^2 \, dA + (\dot{\kappa}_z - \omega \kappa_y) \int\limits_A \beta_{ef} Y_{ef} z^2 \, dA \end{aligned} \tag{3.6}$$

Denote, for convenience, the purely elastic stiffness of the FGM structure by Δ and the term corresponding to viscous effects by B

$$\begin{aligned} \Delta &= \int\limits_A Y_{ef} y^2 \, dA = \int\limits_A Y_{ef} z^2 \, dA \\ B &= \int\limits_A \beta_{ef} Y_{ef} y^2 \, dA = \int\limits_A \beta_{ef} Y_{ef} z^2 \, dA \end{aligned} \tag{3.7}$$

The integration range includes both zones filled with piezoceramic-polymer and polymer-aluminium phases. Thus, the integrals in (3.7) desintegrate into two components each

$$\begin{aligned} \Delta &= \Big(\int\limits_{r_1}^{r_2} Y_{ef1}(r) r^3 \, dr + \int\limits_{r_2}^{r_3} Y_{ef2}(r) r^3 \, dr \Big) \int\limits_0^{2\pi} \sin^2 \varphi \, d\varphi \\ B &= \Big(\int\limits_{r_1}^{r_2} Y_{ef1}(r) \beta_{ef1}(r) r^3 \, dr + \int\limits_{r_2}^{r_3} Y_{ef2}(r) \beta_{ef2}(r) r^3 \, dr \Big) \int\limits_0^{2\pi} \sin^2 \varphi \, d\varphi \end{aligned} \tag{3.8}$$

Knowing that the curvatures κ_y and κ_z are (in the linear approximation) second derivatives of the transverse displacement of the shaft: $\kappa_y = \partial^2 y / \partial x^2$, $\kappa_z = \partial^2 z / \partial x^2$, substituting (3.6) and (3.8) into the equilibrium equations, one arrives at the following equations of motion

$$\begin{aligned} \rho A \frac{\partial^2 y}{\partial t^2} + \Delta \frac{\partial^4 y}{\partial x^4} + B \Big(\frac{\partial^5 y}{\partial x^4 \partial t} + \omega \frac{\partial^4 z}{\partial x^4} \Big) = 0 \\ \rho A \frac{\partial^2 z}{\partial t^2} + \Delta \frac{\partial^4 z}{\partial x^4} + B \Big(\frac{\partial^5 z}{\partial x^4 \partial t} - \omega \frac{\partial^4 y}{\partial x^4} \Big) = 0 \end{aligned} \tag{3.9}$$

or in a dimensionless form

$$\begin{aligned} \frac{\partial^2 \widetilde{y}}{\partial \widetilde{t}^2} + \frac{\partial^4 \widetilde{y}}{\partial \widetilde{x}^4} + \Gamma \Big(\frac{\partial^5 \widetilde{y}}{\partial \widetilde{x}^4 \partial \widetilde{t}} + \Omega \frac{\partial^4 \widetilde{z}}{\partial \widetilde{x}^4} \Big) = 0 \\ \frac{\partial^2 \widetilde{z}}{\partial \widetilde{t}^2} + \frac{\partial^4 \widetilde{z}}{\partial \widetilde{x}^4} + \Gamma \Big(\frac{\partial^5 \widetilde{z}}{\partial \widetilde{x}^4 \partial \widetilde{t}} - \Omega \frac{\partial^4 \widetilde{y}}{\partial \widetilde{x}^4} \Big) = 0 \end{aligned} \tag{3.10}$$

where

$$\begin{aligned} &\widetilde{x} = \frac{x}{l} \qquad \widetilde{y} = \frac{y}{l} \qquad \widetilde{z} = \frac{z}{l} \qquad \widetilde{t} = \frac{t}{k_t} \\ &\Omega = \omega k_t \qquad k_t = l^2 \sqrt{\frac{\rho A}{\Delta}} \qquad \Gamma = \frac{\mathrm{B}}{l^2 \sqrt{\Delta \rho A}} \end{aligned} \tag{3.11}$$

These are, of course, governing equations of the passive FGM system (control disabled) since it lacks the terms describing the performance of actuators. It will be done in forthcoming examinations.

4. Sensor considerations

Consider, in general, a single PVDF ring-shaped thin layer having the anisotropy axes oriented as shown in Fig. 6.

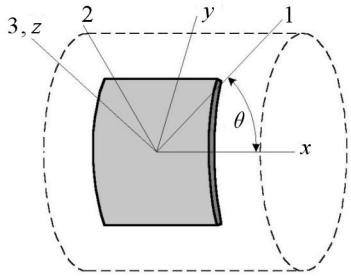

Fig. 6. Sensor layer attached to a shell-like structure

The piezoelectric effect is described by the following constitutive equation (in principal anisotropy axes)

$$D_i = d_{ij}\sigma_j + \epsilon_{ij}E_j \tag{4.1}$$

where D_i is the dielectric displacement, d_{ij} – coefficients of the electromechanical coupling, σ_j – mechanical stress, ϵ_{ij} – dielectric permittivity coefficients, E_j – electric field vector. Assuming the pure direct mechanical-to-electrical conversion effect (excluding presence of any additional electric fields, the so-called eigenfields, see Vasques and Rodrigues, 2005): $\mathbf{E} = \mathbf{0}$ one writes down

$$D_i = d_{ij}\sigma_j \tag{4.2}$$

In a more explicit form the shape of the electromechanical coupling matrix can be observed. The lack of natural shear coefficients is worth mentioning

$$\begin{bmatrix} D_1 \\ D_2 \\ D_3 \end{bmatrix} = \begin{bmatrix} 0 & 0 & 0 & 0 & 0 & 0 \\ 0 & 0 & 0 & 0 & 0 & 0 \\ d_{31} & d_{32} & d_{33} & 0 & 0 & 0 \end{bmatrix} \begin{bmatrix} \sigma_1 \\ \sigma_2 \\ \sigma_3 \\ \sigma_4 \\ \sigma_5 \\ \sigma_6 \end{bmatrix} \tag{4.3}$$

For a thin layer (in-plane stress-strain state: $\sigma_3, \sigma_4, \sigma_5 = 0$)

$$\begin{bmatrix} D_1 \\ D_2 \\ D_3 \end{bmatrix} = \begin{bmatrix} 0 & 0 & 0 \\ 0 & 0 & 0 \\ d_{31} & d_{32} & 0 \end{bmatrix} \begin{bmatrix} \sigma_1 \\ \sigma_2 \\ \sigma_3 \end{bmatrix} \qquad \mathbf{D} = \mathbf{d}\boldsymbol{\sigma} \tag{4.4}$$

Transform now the co-ordinate system $(1, 2, 3)$ into (x, y, z) by rotation around the third axis $3 \equiv z$ by θ

$$\overline{\mathbf{D}} = \overline{\mathbf{d}}\overline{\boldsymbol{\sigma}} \qquad \overline{\boldsymbol{\sigma}} = [\sigma_x, \sigma_y, \tau_{xy}]^\top \tag{4.5}$$

where the overbars are relative to the rotated co-ordinate system:

$$\overline{\mathbf{d}} = \overline{\mathbf{T}}\mathbf{d}\overline{\mathbf{T}}^{-1} \tag{4.6}$$

where $\mathbf{T}$ is the transformation matrix

$$\mathbf{T} = \begin{bmatrix} \cos^2\theta & \sin^2\theta & \sin 2\theta \\ \sin^2\theta & \cos^2\theta & -\sin 2\theta \\ -\dfrac{1}{2}\sin 2\theta & \dfrac{1}{2}\sin 2\theta & \cos 2\theta \end{bmatrix}$$

Moreover

$$\overline{\boldsymbol{\sigma}} = \overline{\mathbf{Q}}\overline{\boldsymbol{\varepsilon}} \Rightarrow \overline{\mathbf{D}} = \overline{\mathbf{dQ}}\overline{\boldsymbol{\varepsilon}} \qquad \overline{\boldsymbol{\varepsilon}} = \left[\varepsilon_x, \varepsilon_y, \frac{1}{2}\gamma_{xy}\right]^\top \tag{4.7}$$

where $\overline{\mathbf{Q}} = \mathbf{TQT}^{-1}$, which entails $\overline{\mathbf{D}} = \mathbf{TdT}^{-1}\mathbf{TQT}^{-1}\overline{\boldsymbol{\varepsilon}} = \mathbf{TdQT}^{-1}\overline{\boldsymbol{\varepsilon}}$. Since PVDFs are poled in the 3-rd direction, the electrodes must be attached to the normal surfaces. Therefore, the dielectric displacement (and the resulting charge) is of the greatest interest

$$\overline{D}_3 = D_3 = D_z = \{\mathbf{TdQT}^{-1}\}_3\overline{\boldsymbol{\varepsilon}} = [\Delta_1, \Delta_2, \Delta_3] \cdot \left[\varepsilon_x, \varepsilon_y, \frac{1}{2}\gamma_{xy}\right]^\top \tag{4.8}$$

A single PVDF sensor patch is glued to the surface of each structure shown in Fig. 7.

The structure can be subject to a combination of the following vibration modes: transverse vibration due to radial motion (pure swelling in the radial direction), transverse vibration due to bending, and torsional vibration (twisting). Find now, how effective can be the PVDF sensor in measuring each of the indicated vibration types.

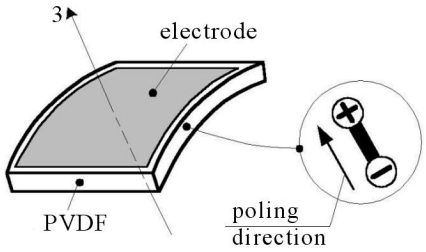

Fig. 7. Polarisation of a PVDF film

Let the sensor be a small rectangular patch bonded to the host structure as shown in Fig. 8. This time (pure bending) the strain vector assumes the form: $\overline{\varepsilon} = [\varepsilon_x, 0, 0]$, and the dielectric displacement in the 3-rd (z) axis is

$$D_3 = [\Delta_1, \Delta_2, \Delta_3] \begin{bmatrix} \varepsilon_x \\ 0 \\ 0 \end{bmatrix} = \Delta_1 \varepsilon_x \tag{4.9}$$

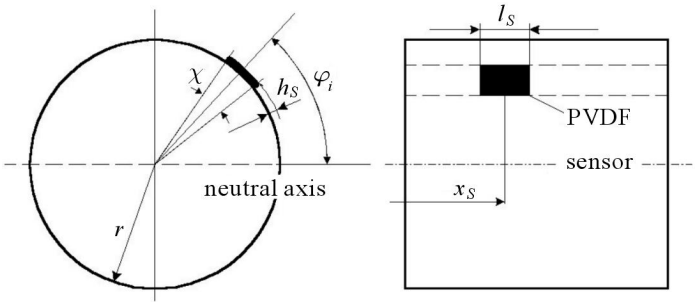

Fig. 8. Model of the sensors for measuring bending modes

The electric charge and the resulting voltage on the ith sensor patch will be

$$\begin{aligned} q_{3i} &= \int\limits_A D_3 \, dA_i = \Delta_1 r^2 \int\limits_{x_s - \frac{l_s}{2}}^{x_s + \frac{l_s}{2}} \kappa(x) \, dx \int\limits_{\varphi_i - \frac{\chi}{2}}^{\varphi_i + \frac{\chi}{2}} \sin\varphi \, d\varphi \\ U_{Si} &= \frac{q_{3i}}{C} = \frac{\Delta_1 h_s r}{\epsilon_s \chi l_s} \int\limits_{x_s - \frac{l_s}{2}}^{x_s + \frac{l_s}{2}} \kappa(x) \, dx \Big[\cos\Big(\varphi_i - \frac{\chi}{2}\Big) - \cos\Big(\varphi_i + \frac{\chi}{2}\Big) \Big] \end{aligned} \tag{4.10}$$

where κ denotes the curvature: $\kappa = \partial^2 w/\partial x^2$, the substitution of which entails

$$U_{Si} = \frac{\Delta_1 h_s r}{\epsilon_s \chi l_s}\Big[\frac{\partial w\Big(x_s + \frac{l_s}{2}\Big)}{\partial x} - \frac{\partial w\Big(x_s - \frac{l_s}{2}\Big)}{\partial x}\Big] 2\sin\varphi_i \sin\frac{\chi}{2} \tag{4.11}$$

As it can be seen, the produced voltage is directly proportional to the difference between the slopes at the beginning and ending points of the sensor patch. For very small sensor elements (both in the radial and longitudinal directions), equation (4.11) can be rewritten as follows

$$U_{Si} = \lim_{\substack{l_s \to 0 \\ \chi \to 0}} U_S(l_s, \chi) = \frac{\Delta_1 h_s r}{\epsilon_s} \frac{\partial^2 w(x_s)}{\partial x^2} \sin\varphi_i \tag{4.12}$$

Again, the term Δ_1 strongly depends on the geometric configuration of the attached sensor. This dependence is shown in Fig. 9.

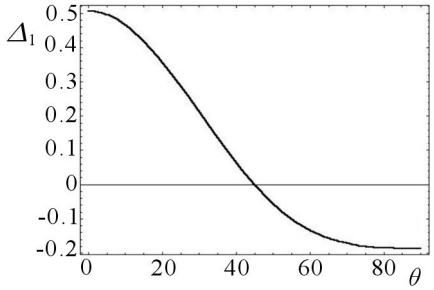

Fig. 9. Efficiency of voltage generation for bending vibration modes vs. orientation of the PVDF sensing patch

As it can be seen, the most favourable geometric orientation of the PVDF sensing patches is for $\theta = 0°$. Then

$$U_{Si} = \frac{\Delta_1(0°) h_s r}{\epsilon_s} \frac{\partial^2 w(x_s)}{\partial x^2} \sin\varphi_i \tag{4.13}$$

or briefly

$$U_{Si} = \gamma_S \frac{\partial^2 w(x_s)}{\partial x^2} \sin\varphi_i \tag{4.14}$$

5. Control of the rotating FGM structure

Consider now the problem of control of transverse vibration of a rotating shaft made of a Functionally Graded Material comprising an active piezoce-

ramic (PZT) fraction. Let us analyse a single electrode covering a part of the shaft circumference as shown in Fig. 10.

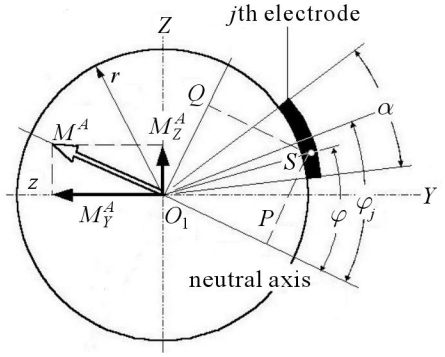

Fig. 10. Electrode patch controlling a sector of piezoceramic structure

According to the converse law of piezoelectricity (Nye, 1985), the stress generated within a piezoelectric gradient structure is

$$\sigma = Y_{ef}(\varepsilon - d_{31}^{ef} E_3) \tag{5.1}$$

where Y_{ef} denotes the effective Young's modulus, ε – strain, d_{31}^{ef} – effective electromechanical coupling constant, E_3 – applied electric field. Integrating the terms of stress purely related to d_{31}^{ef} one can write down (see also Fig. 5)

$$M_{Ai} = -\int_A PS \cdot Y_{ef} d_{31}^{ef} E_{3i}\, dA \tag{5.2}$$

It is a bending moment produced by the ith electrode, contributing to the entire moment controlling the shaft. Putting it down more explicitly, one finds:

$$M_{Ai} = -E_{3i} \int_{r_1}^{r_2} Y_{ef1}(r) d_{31}^{ef}(r) r^2\, dr \int_{\varphi_i - \frac{\alpha}{2}}^{\varphi_i + \frac{\alpha}{2}} \sin\varphi\, d\varphi = -E_{3i} \Xi \sin\varphi_i \tag{5.3}$$

where the introduced constant is

$$\Xi = 2 \sin\frac{\alpha}{2} \int_{r_1}^{r_2} Y_{ef1}(r) d_{31}^{ef}(r) r^2\, dr \tag{5.4}$$

and the electric field results from the applied voltage and the distance between the electrodes, see Fig. 1

$$E_{3i} = \frac{U_{Ai}}{r_2 - r_1} \tag{5.5}$$

It is here assumed that the electric field is constant through the shaft thickness, which is only a simplification of real electrical conditions. Admittedly, the electric field intensity does not behave as a constant quantity since the dielectric permittivity varies with radius due to the gradual change of contacting component (having, naturally, different values of ϵ_i), see Tylikowski and Przybyłowicz (2004).

Obviously, the voltage itself follows the incorporated control law, which is here based on a differential regulator. Hence

$$U_{Ai} = k_d \frac{dU_{Si}}{dt} \tag{5.6}$$

where k_d is the gain factor. Substituting the equation describing the voltage generated in the ith single sensor supplying signals to the ith electrode via the control unit, see Eqs (4.13) and (4.14), one obtains

$$\begin{aligned} E_{3i} &= \frac{k_d}{r_2 - r_1} \frac{d}{dt}\Big(\gamma_S \frac{\partial w(x_S)}{\partial x^2} \sin\varphi_i\Big) = \\ &= \frac{k_d}{r_2 - r_1} \gamma_S \Big(\frac{\partial \dot{w}(x_S)}{\partial x^2} \sin\varphi_i + \omega \frac{\partial w(x_S)}{\partial x^2} \cos\varphi_i\Big) \end{aligned} \tag{5.7}$$

And the ith bending moment

$$M_{Ai} = \frac{k_d}{r_2 - r_1} \gamma_S \Xi \Big(\frac{\partial \dot{w}(x_S)}{\partial x^2} \sin^2\varphi_i + \omega \frac{\partial w(x_S)}{\partial x^2} \sin\varphi_i \cos\varphi_i\Big) \tag{5.8}$$

Decomposing the thus determined moment into two directions y and z, one reads

$$\begin{pmatrix} M_{Ai}^z \\ M_{Ai}^y \end{pmatrix} = \gamma_d(n) \left\{ \begin{pmatrix} \dfrac{\partial^3 y(x_S)}{\partial x^2 \partial t} \\ \dfrac{\partial^3 z(x_S)}{\partial x^2 \partial t} \end{pmatrix} \sin^2\varphi_i + \frac{\omega}{2} \begin{pmatrix} \dfrac{\partial^2 y(x_S)}{\partial x^2} \\ \dfrac{\partial^2 z(x_S)}{\partial x^2} \end{pmatrix} \sin 2\varphi_i \right\} \tag{5.9}$$

where γ_d stands for the general coefficient shortly expressing the multiplier $k_d \gamma_S \Xi/(r_2 - r_1)$. It is here underlined that this factor depends on the applied function of volume distribution of the active piezoceramic fraction in the FGM structure, described by the exponent n: $\gamma_d = \gamma_d(n)$.

The resultant controlling moment will be

$$M_A^{(z,y)} = \sum_{i=1}^{N} M_{Ai}^{(z,y)} \tag{5.10}$$

where N is the number of electrodes placed around the shaft perimeter. Note, that the angular distance between the jth and $(j+1)$th electrode is $\varphi_{j+1} - \varphi_j = 2\pi/n$. Denoting the position of the first pair of electrodes by $\varphi_1 = \varphi$, one finds locations of the subsequent electrodes

$$\varphi_k = \varphi + \frac{2\pi k}{N} \tag{5.11}$$

Now analyse the sums involving expressions of the angular position φ_j in (5.10). According to (5.9), there are two such sums

$$\sum_{k=1}^{N} \sin^2 \varphi_k = \sum_{k=1}^{N} \sin^2\Big(\varphi_k + k\frac{2\pi}{N}\Big) = \begin{cases} \sin^2 \varphi & \text{for} \quad N = 1 \\ 2\sin^2 \varphi & \text{for} \quad N = 2 \\ \dfrac{N}{2} & \text{for} \quad N \geqslant 3 \end{cases}$$

$$\sum_{k=1}^{N} \sin \varphi_k \cos \varphi_k = \frac{1}{2}\sum_{k=1}^{N} \sin 2\Big(\varphi_j + k\frac{2\pi}{N}\Big) = \begin{cases} \dfrac{1}{2}\sin 2\varphi & \text{for} \quad N = 1 \\ \sin 2\varphi & \text{for} \quad N = 2 \\ 0 & \text{for} \quad N \geqslant 3 \end{cases} \tag{5.12}$$

It is clearly seen that application of 3 or more electrode patches ensures generation of a constant bending moment (non-oscillating), which is a very desired and advantageous effect making the control of the rotating structure quite convenient.

Finally, the vector of actuating moment assumes the form

$$\boldsymbol{M}_A = \gamma_d(n)\frac{N}{2}\begin{bmatrix} \dfrac{\partial^3 y(x_S)}{\partial x^2 \partial t} \\ \dfrac{\partial^3 z(x_S)}{\partial x^2 \partial t} \end{bmatrix} \{H(x) - H(x-l)\} \tag{5.13}$$

The presence of Heaviside's step functions $H(\cdot)$ results from the fact that the electrodes may not necessarily cover the entire length of the shaft, but only a part of it, e.g. between $x = x_1$ and $x = x_2$. Here it is assumed that $x_1 = 0$ and $x_2 = l$. The second derivative of $\boldsymbol{M}_A$ present in the equations of motion becomes

$$\frac{\partial^2 \boldsymbol{M}_A}{\partial x^2} = c_d(n)\begin{bmatrix} \dfrac{\partial^3 y(x_S)}{\partial x^2 \partial t} \\ \dfrac{\partial^3 z(x_S)}{\partial x^2 \partial t} \end{bmatrix} \Big\{\frac{\partial \delta(x)}{\partial x} - \frac{\partial \delta(x-l)}{\partial x}\Big\} \tag{5.14}$$

where $c_d = \gamma_d N/2$ and $\delta(\cdot)$ is the Dirac Delta function.

6. Stability investigations

Having derived the resultant bending moment generated within the active piezoelectric fraction, see (5.14), one substitutes it into equations of motion (3.10), which leads to (in a dimensionless form)

$$\begin{aligned}
&\frac{\partial^2\widetilde{y}}{\partial\widetilde{t}^2}+\frac{\partial^4\widetilde{y}}{\partial\widetilde{x}^4}+\Gamma\Big(\frac{\partial^5\widetilde{y}}{\partial\widetilde{x}^4\partial\widetilde{t}}+\Omega\frac{\partial^4\widetilde{z}}{\partial\widetilde{x}^4}\Big)-\widetilde{c}_d(n)\frac{\partial^3\widetilde{y}(\widetilde{x}_S)}{\partial\widetilde{x}^2\partial\widetilde{t}}\Big(\frac{\partial\delta(\widetilde{x})}{\partial\widetilde{x}}-\frac{\partial\delta(\widetilde{x}-1)}{\partial\widetilde{x}}\Big)=0\\
&\frac{\partial^2\widetilde{z}}{\partial\widetilde{t}^2}+\frac{\partial^4\widetilde{z}}{\partial\widetilde{x}^4}+\Gamma\Big(\frac{\partial^5\widetilde{z}}{\partial\widetilde{x}^4\partial\widetilde{t}}-\Omega\frac{\partial^4\widetilde{y}}{\partial\widetilde{x}^4}\Big)-\widetilde{c}_d(n)\frac{\partial^3\widetilde{z}(\widetilde{x}_S)}{\partial\widetilde{x}^2\partial\widetilde{t}}\Big(\frac{\partial\delta(\widetilde{x})}{\partial\widetilde{x}}-\frac{\partial\delta(\widetilde{x}-1)}{\partial\widetilde{x}}\Big)=0
\end{aligned}\tag{6.1}$$

In order to examine dynamic stability of the analysed system, equations of motion (6.1) will be transformed into a set of ordinary differential equations by making use of a unimodal Galerkin's discretisation based on the first eigenform corresponding to a simply supported beam. Let (6.1) be represented in the form of differential operators $\Im_i[\widetilde{y}(\widetilde{x},\widetilde{t}),\widetilde{z}(\widetilde{x},\widetilde{t})]$, $i=1,2$. Let the solution to (6.1) be predicted as $\widetilde{y}(\widetilde{x},\widetilde{t})=T_1(\widetilde{t})F(\widetilde{x})$ and $\widetilde{z}(\widetilde{x},\widetilde{t})=T_2(\widetilde{t})F(\widetilde{x})$ where $F(\widetilde{x})=\sin(\widetilde{x})$ and $T_1(\widetilde{t})$, $T_2(\widetilde{t})$ are arbitrary time functions. The Galerkin discretisation implies

$$\int_0^1 \Im_i\Big\{\widetilde{y}[(F(\widetilde{x})T_1(\widetilde{t})],\widetilde{z}[(F(\widetilde{x})T_2(\widetilde{t})]\Big\}F(\widetilde{x})\,d\widetilde{x}=0\qquad i=1,2 \tag{6.2}$$

which leads to a set of two second-order ordinary differential equations with respect to T_1 and T_2

$$\begin{aligned}
&\ddot{T}_1\int_0^1 F^2\,d\widetilde{x}+[T_1+\Gamma(\dot{T}_1+\Omega T_2)]\int_0^1 FF^{IV}\,d\widetilde{x}+\\
&-\widetilde{c}_d\dot{T}_1\int_0^1 F^{II}(\widetilde{x}_S)[\delta^I(\widetilde{x})-\delta^I(\widetilde{x}-1)]F\,d\widetilde{x}=0\\
&\ddot{T}_2\int_0^1 F^2\,d\widetilde{x}+[T_2+\Gamma(\dot{T}_2-\Omega T_1)]\int_0^1 FF^{IV}\,d\widetilde{x}+\\
&-\widetilde{c}_d\dot{T}_2\int_0^1 F^{II}(\widetilde{x}_S)[\delta^I(\widetilde{x})-\delta^I(\widetilde{x}-1)]F\,d\widetilde{x}=0
\end{aligned}\tag{6.3}$$

Taking into account fundamental properties of the eigenfunction $F(\widetilde{x})$, i.e. knowing that

$$\int_0^1 F^2(\widetilde{x})\,d\widetilde{x} = \frac{1}{2} \qquad \int_0^1 F(\widetilde{x})F^{IV}(\widetilde{x})\,dx = \frac{\pi^4}{2} \tag{6.4}$$

and making use of the fact that for any function $f(x)$ the following holds

$$\int_0^1 f(x)\frac{d\delta(x-x_S)}{dx}\,dx = -\frac{df(x_S)}{dx} \qquad \text{if } \; 0 < x_S < 1 \tag{6.5}$$

one arrives at the final form of the discretised equations of motion

$$\begin{aligned} \ddot{T}_1 + \pi^4[T_1 + \Gamma(\dot{T}_1 + \Omega T_2) - c_d\dot{T}_1] = 0 \\ \ddot{T}_2 + \pi^4[T_2 + \Gamma(\dot{T}_2 - \Omega T_1) - c_d\dot{T}_2] = 0 \end{aligned} \tag{6.6}$$

where the tilde over gain c_d has been omitted for convenience. Transforming (6.6) into four differential equations of the first order by substituting new variables: $u_1 = T_1$, $u_2 = \dot{T}_1$, $u_3 = T_2$, $u_4 = \dot{T}_2$, a newly obtained form of governing formulas is

$$\begin{bmatrix} \dot{u}_1 \\ \dot{u}_2 \\ \dot{u}_3 \\ \dot{u}_4 \end{bmatrix} = \begin{bmatrix} 0 & 1 & 0 & 0 \\ -\pi^4 & -\pi^4\Gamma + c_d & -\Gamma\Omega\pi^4 & 0 \\ 0 & 0 & 0 & 1 \\ \Gamma\Omega\pi^4 & 0 & -\pi^4 & -\pi^4\Gamma + c_d \end{bmatrix} \begin{bmatrix} u_1 \\ u_2 \\ u_3 \\ u_4 \end{bmatrix} \tag{6.7}$$

or shortly

$$\dot{\boldsymbol{u}} = \mathbf{A}(c_d)\boldsymbol{u}$$

Proceed now with the stability analysis. The system remains stable as long as real parts of all eigenvalues corresponding to the matrix $\mathbf{A}(c_d)$ are negative. Find then the eigenvalues by formulating the eigenproblem

$$\det\{\mathbf{A}(c_d) - s\mathbf{I}\} = 0 \tag{6.8}$$

which yields two conjugate pairs of complex eigenvalues

$$\begin{aligned} s_1 &= \zeta_1 + \mathrm{i}\eta_1 & s_2 &= \overline{r}_1 = \zeta_1 - \mathrm{i}\eta_1 \\ s_3 &= \zeta_2 + \mathrm{i}\eta_2 & s_4 &= \overline{r}_3 = \zeta_2 - \mathrm{i}\eta_2 \end{aligned} \tag{6.9}$$

Concentrate now on the eigenvalue having the greatest real part. It is the decisive eigenvalue, and let it be denoted by s_1. Then the system is said to be stable if $\mathrm{Re}\{s_1\} < 0$.

Some exemplary trajectories of the decisive eigenvalue are presented in Fig. 11 for growing rotation speed of the shaft and for selected gain factors in the control unit. The eigenvalue moves rightwards with increasing rotation speed. It starts from the area where $\mathrm{Re}\{s_1\} < 0$, then it intersects the imaginary axis, and finally its real part becomes positive. This exactly entails the loss of stability and initiates a self-excited flutter-type vibration. The ordinate, i.e. imaginary part, corresponds to the initial frequency of such vibration. As at can be seen, the enabled control $(c_d \neq 0)$ moves the trajectories leftwards, i.e. stabilises the system.

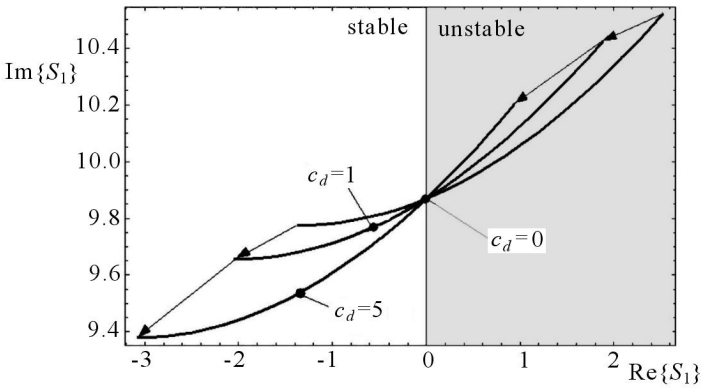

Fig. 11. Trajectories of the decisive eigenvalue for some gain factors

A clearer view on the stabilising effect is presented in Fig. 12. The increase of the critical rotation speed with growing c_d is easily visible there for a few chosen exponents n describing the type of volume distribution of active and passive constituents of the FGM structure.

Growing number n means, of course, faster transition between two mixing phases in favour the active PZT fraction. Thus, the lines $\Omega_{cr} = \Omega_{cr}(n)$ in Fig. 12 get steeper for higher n. Admittedly, n cannot be freely lifted up since it would inevitably lead to disappearance of gradual change of electromechanical properties within the employed FGM and to a considerable concentration of stress.

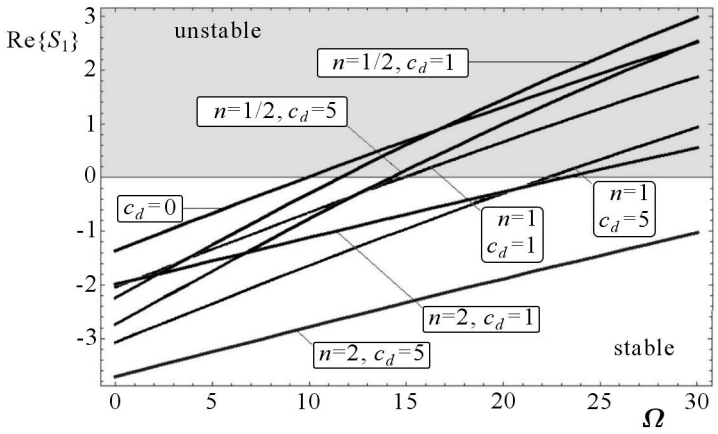

Fig. 12. Real part of the decisive eigenvalue for different gain factors and exponential functions describing the volume distribution of the active PZT fraction

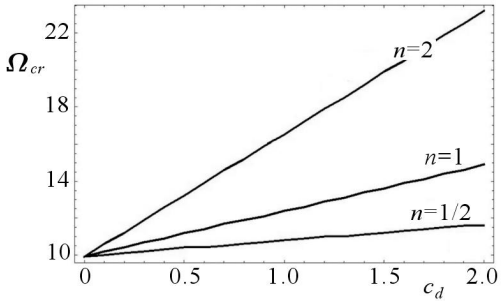

Fig. 13. Critical rotation speed vs. gain for selected exponents of the PZT-volume distribution function

7. Concluding remarks

In this paper, fundamentals of active stabilisation of transverse vibration of a rotating shaft have been presented. The applied method of stabilisation, based on making use of a functionally graded material that involves an active piezoceramic fraction, proves to be an efficient solution to the analysed problem. An FGM shaft remains both stiff thanks to the passive metallic component and controllable owing to the active PZT phase. Moreover, it occurs that the application of only three actuating electrodes around the shaft perimeter is enough to produce a constant counter-bending moment despite rotary motion of the entire structure. Such a moment opposes internal interactions due to internal friction that lead to self-excitation while exceeding the critical angular velocity.

It is to be emphasized that distributions of the volume share of the active component (described by various numbers of the exponent n) highly affect the mentioned efficiency. One can observe evident growth of the critical rotation speed with n. Still interesting, regardless of the fact whether the system is controlled or not, the initial self-excitation frequency remains the same: $\mathrm{Im}\{s_1(c_d)\} = \mathrm{const}$. Great values of the exponents, however, such as $n = 10$ and more, make the FGM shaft structure no longer graded but a three-layer laminate-like with distinctly separated phases. That would directly lead to rapid stress concentrations near the contact areas between these phases, which is obviously in pure opposition to the concept of a functionally graded structure. Distributions with $n \approx 5$ seem to be the most reasonable compromise, see Fig. 14.

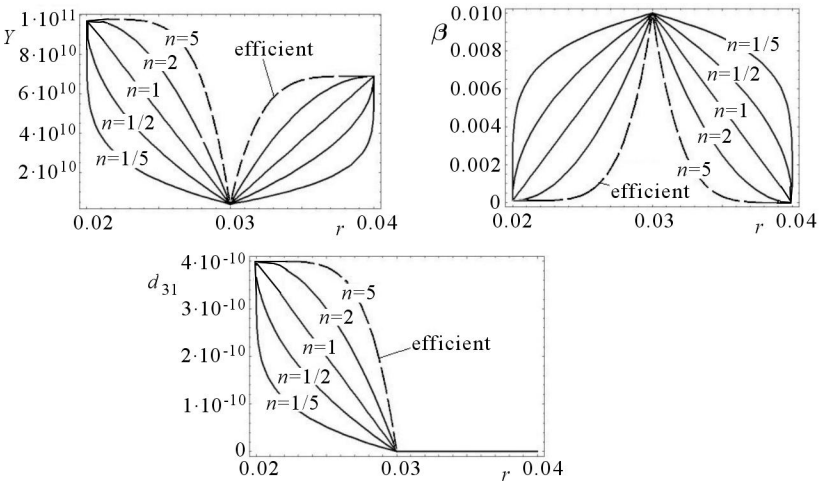

Fig. 14. A reasonable choice of effective Young's modulus, internal damping and electromechanical coupling constant (broken lines) distributed throughout the graded structure

Acknowledgement

This work has been done as a part of the research project No. 5 T07C 010 25 supported by the State Committee for Scientific Research (KBN), which is gratefully acknowledged by the author.

References

1. KURNIK W., 1992, Hysteretic behaviour of a rotating shaft with geometric and physical nonlinearities, *Zeitschrift fr Angewandte Mathematik und Mechanik*, **72**, 4, T37-T75

2. KURNIK W., PRZYBYŁOWICZ P.M., 2003, Active stabilisation of a piezoelectric fiber composite shaft subjected to follower load, *International Journal of Solids and Structures*, **40**, 5063-5079

3. LIBRESCU L., SANG-YONG OH, OHSEOP SONG, 2005, Thin-walled beams of functionally graded materials and operating in a high temperature environment: vibration and stability, *Journal of Thermal Stresses*, **28**, 649-712

4. LIEW K.M., SIVASHANKER S., HE X.Q., NG T.Y., 2003 The modelling and design of smart sructures using functionally graded material and piezoelectric sensor/actuator patches, *Smart Materials and Structures*, **12**, 647-655

5. NEWNHAM R.E., BOWEN K.A., KLICKER K.A., CROSS L.E., 1980, Composite piezoelectric transducers, *Material Engineering*, **2**, 93-106

6. NYE J.F., 1985, *Physical Properties of Crystals*, Oxford: Clarendon

7. PRZYBYŁOWICZ P.M., 2002a, Near-critical behaviour of a rotating shaft actively stabilised by piezoelectric elements, *Systems Analysis Modelling Simulation*, **42**, 4, 527-537

8. PRZYBYŁOWICZ P.M., 2002b, Stability of rotating shafts made of piezoelectric fiber composites, *Journal of Theoretical and Applied Mechanics*, **40**, 4, 1021-1049

9. SAFARI A., 1999, Novel piezoelectric ceramics and composites for sensor and actuator applications, *Materials Research Innovations*, **2**, 263-269

10. TYLIKOWSKI A., 2001, Piezoelektryczne materiały gradientowe i ich zastosowanie w aktywnym tłumieniu drgań, *V Szkoła „Metody Aktywne Redukcji Drgań i Hałasu"*, Akademia Górniczo Hutnicza, Kraków-Krynica, 285-290

11. TYLIKOWSKI A., PRZYBYŁOWICZ P.M., 2004, *Nieklasyczne materiały piezoelektryczne w stabilizacji i tłumieniu drgań*, Wyd. Instytut Podstaw Budowy Maszyn Politechniki Warszawskiej

12. VASQUES C.M.A., RODRIGUES J.D., 2005, Coupled three layered analysis of smart piezoelectric beams with different electric boundary conditions, *International Journal for Numerical Methods in Engineerin*, **62**, 11, 1488-1518

Stateczność wirującego wału wykonanego z materiału gradientowego

Streszczenie

W pracy przedstawiono zagadnienie aktywnej stabilizacji wirującego wału wykonanego z trójfazowego materiału gradientowego (FGM) zawierającego składnik piezoelektryczny. Niezależnie od zastosowanego materiału, obecność tarcia wewnętrznego powoduje utratę stateczności wału i powstanie drgań samowzbudnych przy pewnej krytycznej prędkości wirowania. W artykule przedyskutowano sposób zapobiegania takiemu zjawisku oparty na zastosowaniu materiału gradientowego FGM sterowanego napięciem elektrod przyklejonych i zatopionych w strukturze wału. Wartość krytycznej prędkości wirowania znaleziono poprzez badanie wartości własnych równań ruchu zlinearyzowanych po jednomodalnej dyskretyzacji Galerkina równań różniczkowych cząstkowych. Głównym celem analizy jest określenie optymalnego rozkładu funkcji opisującej objętościowy udział aktywnej frakcji piezoelektrycznej w użytym materiale FGM, który zapewnia możliwie najlepszy efekt stabilizacyjny i równocześnie utrzymuje dobre właściwości wytrzymałościowe wału. Rezultaty badań przedstawiono na wykresach pokazujących krytyczną prędkość wirowania w funkcji wykładnika opisującego rozkład udziału objętościowego fazy aktywnej oraz współczynników wzmocnienia zastosowanych w układzie sterowania.

Manuscript received March 5, 2005; accepted for print May 23, 2005